UNIVERSITY OF CALIFORNIA

Los Angeles

Impact of Ozone Exposure on OPV Efficiency

A thesis submitted in partial satisfaction

of the requirements for the degree Master of Science

in Materials Science and Engineering

by

Aneeket Jaisukhlal Palankar

2017

ABSTRACT OF THE THESIS

Impact of Ozone Exposure on OPV Efficiency

by

Aneeket Jaisukhlal Palankar

Master of Science in Materials Science and Engineering

University of California, Los Angeles, 2017

Professor Yang Yang, Chair

Organic solar cells are a considerable promise for alternate energy sources owing to their plentiful, easily accessible and renewable source of power. Degradation on organic film and anode layer are the major factors that determine device reliability and ozone can induce damage to these materials due to its strong oxidizing property. This study measured the sustainability of a type of organic photovoltaic (OPV) film (P3HT:$PC_{71}BM$) and its anodes (Al and MoO_3) to different levels of ozone environment and investigated the impact of ozone exposure on OPV film and anodes efficiency. The devices were fabricated in a Glove Box under controlled N_2 atmosphere using Spin Coating and Physical Vapor Deposition and exposed to varied ozone concentrations, followed by J-V measurements to determine the Power Conversion Efficiency and Fill Factor. The effects of ozone exposure on the films were compared vs. the effects of exposure on complete devices with anodes (Al and MoO_3). The results show that the devices

decay from normal efficiency (4%) to 0% in 12 hours under 300 ppb (±10%) ozone concentration and decay to 0% in 6 hours when the ozone concentration was 600 ppb (±10%), when only the polymer thin films are exposed. This established an inverse linear relationship between the decay rate and ozone exposure at high concentrations on the OPV films. Furthermore, the effect of exposure to ambient ozone concentration on the polymer films, which is 70 ppb (±15%), was also investigated and the devices were found to decay to 0% in 28 hours, which is much faster than expected. The decay resistance of complete devices when the polymer films are coated with thermally evaporated anodes (Al and MoO_3) before exposure to 400 ppb ozone concentration was investigated. The average efficiency of the complete device after 2, 6, 10, 15, 28 and 42 hours exposure in 400 ppb ozone environment was 4.16% with a standard deviation of 0.12%. The test findings for the complete device with coated anodes show that the current design of the complete OPV device has good resistance to ozone oxidation without additional protection or encapsulation. This finding has significant bearing with respect to the selection and price of encapsulation material requirements for OPV. This research work is a part of a project funded by the National Science Foundation (Grant # CHE – 1230598) on the SEP Collaborative: Development of economically viable, highly efficient organic photovoltaic solar cells.

The thesis of Aneeket Jaisukhlal Palankar is approved.

Mark S. Goorsky

Jenn-Ming Yang

Yang Yang, Committee Chair

University of California, Los Angeles

2017

Table of Contents

List of Figures

List of Tables

List of Abbreviations

OPV	Organic Photo-voltaic
PVD	Physical Vapor Deposition
P3HT	Poly(3-hexylthiophene)
$PC_{71}BM$	Phenyl-C71-butyric acid methyl ester
BHJ	Bulk Heterojunction
AM 1.5	Air Mass 1.5
PCE	Power Conversion Efficiency
FF	Fill Factor
PAL	Photoactive Layer
J_{sc}	Short Circuit Current Density
V_{oc}	Open Circuit Voltage
QE	Quantum Efficiency
I_{sc}	Short Circuit Current
PPV	Poly(p-phenylenevinylene)
MEH-PPV	Poly(2-methoxy-5-(2'-ethyl-hexyloxy)-1,4-phenylenevinylene
P3AT	Poly(3-alkylthiophene)
P3OT	Poly(3-octylthiophene)

Acknowledgments

I would like to express my deepest and sincerest appreciation to my advisor, Dr. Yang Yang, for his support during my graduate education. This work wouldn't have been possible without his guidance.

I would like to express my gratitude to my mentors, Prof. Gang Li and Dr. En-Ping Yao for their tremendous support, guidance throughout this project and for training me on various instruments and skills necessary to carry out this research. I am sure these skills would be beneficial to me throughout my life. I am highly obliged to my fellow lab mates Huajun Chen, Sheng-Yung Chang, Zhanlue Yang and Bowen Xuan for their impactful insights and valuable suggestions regarding my research work. I owe great gratitude to the entire YY Lab team for their assistance during my research.

I would also like to thank Dr. Peter Sinsheimer and Tianyang Wang for helping me with the ozone exposure treatment and their insights into the degradation behavior of the devices. I am grateful to Dr. Bruce S. Dunn and Dr. Leland Smith for allowing me to use the FTIR instrument for my research and their guidance.

This work was financially supported by a grant from the National Science Foundation (Grant # CHE - 1230598).

1 Introduction

1.1 Motivation

The cost of electricity needed to make solar technologies comparable with the conventional sources of electricity generation is about 5¢/ kWh. When it comes to OPV technology, the materials needed to build these devices are economically viable and highly efficient, besides having easier and cheaper processing techniques, especially when it comes to conjugated polymers. But they do not have the comparable stability of inorganic solar cells. The assumption of an OPV device having 5% efficiency with a life-time of 5 years yields a levelized electricity cost (LEC) in the range of 49¢/ kWh to 85¢/ kWh. Given that the technology is very young, the LEC range is very large but nowhere competitive to the conventional sources of electricity. But, if an efficiency of 15% and a life-time of 20 years is assumed, the LEC range is narrowed down to 7¢/ kWh and 13¢/ kWh [1]. A number of studies have been carried out denoting the susceptibility of organic materials to degradation by oxygen and water, compared to inorganic materials, but the degradation mechanisms are not clearly understood. UV illumination readily activates oxygen when sensitizers like organic molecules or titanium oxide are present. The active polymers or any organic substance present is then attacked by this superoxide or hydrogen peroxide thus formed. Diffusion of oxygen and water into the device is possible through certain thin films. Also, this diffusion may occur via the microscopic pinholes present on the surface of outer electrodes and these aren't the only diffusion channels present on evaporated electrodes. Oxidation and expansion of the organic material in all direction leads to swelling on the outer electrode, which is centered around the microscopic pinholes on the electrode surface. The degradation of the photoactive layer (PAL) is caused by such degradation of the electrode

surface since the voids and insulating patches formed decrease the interfacial area. Hence, the charge transfer between the photoactive layer and electrodes deteriorates. Conductivity of thin film reduces upon exposure to oxygen since it acts as an electron trap hence, reduces the electron mobility by several orders of magnitude. Ordering of the polymer chains is affected due to the increase in permeability and decrease in mobility and permeability is influenced by both, the interaction strength with the penetrant as well as the mobility of polymer chains. Permeability and mobility are also affected by chain scission, since it leads to an increase in the polymer free volume. This compound effect on the polymer ordering affects charge transport and hence causes cell degradation. OPV cell efficiency drop is induced by the decrease in short circuit current density (J_{sc}) as a result of these factors [2]. In order to maintain OPV life-time and stability, solutions to these reliability issues have to be investigated and Ozone effect in OPV is a brand new direction in the field. It is also an important aspect in OPV application involving both energy and environmental impact.

1.2 Objective

The aim of this thesis is to investigate stability of P3HT:$PC_{71}BM$ (OPV) solar devices under ozone exposure. Ozone is one of the six criteria air pollutants regulated by the Clean Air Act, and is currently a major environmental problem in California. In 2016, the National Ambient Air Quality Standards for ozone have been updated to 70 ppb. Besides numerous adverse health impacts, ozone can also induce damages to materials because of its strong oxidizing property. Hence, the effect of ozone exposure on the polymer films at different concentrations, including ambient condition is investigated and compared with the effect of exposure on complete device (after coating anode layers). The relationship between decay rate of the devices, time and

strength of exposure is established. Lastly, robustness and resistance of anode materials (Al and MoO_3) is demonstrated.

2 Background

2.1 Organic Photovoltaics (OPV) – History and Concept

Thin film organic semiconducting polymers form the basis of OPV technology. These polymers have the combination of optoelectronic properties of conventional semiconductors as well as comparatively easier and excellent processing and mechanical properties. Also, the molecular properties can be tailored as per the required application. The polymer processing can be done at room temperature from solutions onto flexible substrates using Spin Coating, which is a very cheap deposition method. Besides, these devices have low materials requirements and the materials utilized are eco-friendly in addition to the reduced production energy and effort needed. Recent progress in this field has been achieved by using organic mono-crystalline, multilayered thin films and interpenetrated network technologies. Hence, OPVs have the potential of a very fast increase in Power conversion efficiency and Fill factor. The Bulk heterojunction structure boosted the external quantum efficiencies (EQE) by 50%, while conjugated polymers and fullerene blends have boosted it to 80% [2]. Fig. 2.2 depicts the PCE increase in OPV solar cells during the past decade.

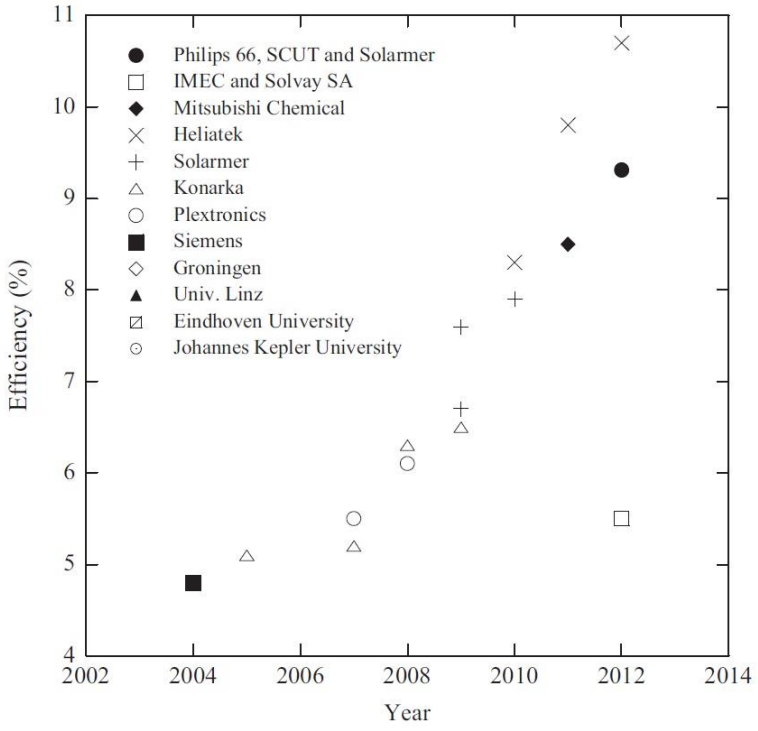

Figure 2.1: Advancement of maximum OPV cell efficiency over the past decade [2]

Semiconducting properties in common dyes like methylene blue were discovered in the early 1960s, later becoming the first organic materials to show PV effect. Carotenes, chlorophylls, porphyrins and phthalocyanines, which are all important biological molecules, showed the PV effect.

Organic solar cells have a planar layered structure. Earlier designs consisted of two different electrodes that sandwiched the light-absorbing or photoactive layer. Aluminum, calcium, magnesium or gold are used as one electrode and the other is generally Indium-tin-oxide (ITO), since it has to be semi-transparent. When light is absorbed, an exciton is formed. This happens because an electron is promoted to the lowest unoccupied molecular orbital (LUMO) from the highest occupied molecular orbital (HOMO). Next, dissociation of the exciton happens, which is basically the electron and hole reaching separate electrodes and this process needs the assistance

of an electrical field. The asymmetrical ionization potential/ work-function of the electrodes take care of this electrical field required while also favoring electron-flow from the low work-function electrode to the high work-function electrode, which is also known as rectification (Forward Bias). Fig. 2.4 shows the energy level positions along with the light harvesting process.

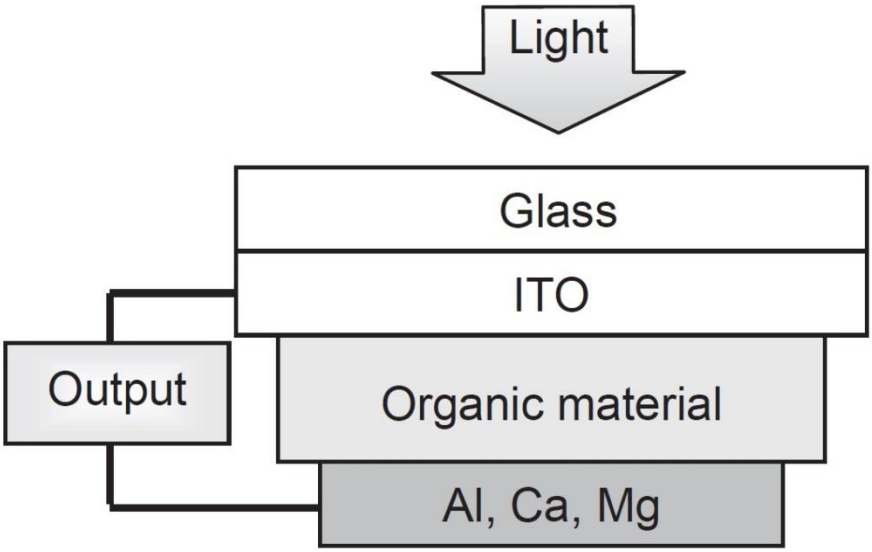

Figure 2.2: Typical PV device. The electrons are collected at the metal electrode and the holes are collected at the ITO electrode [3]

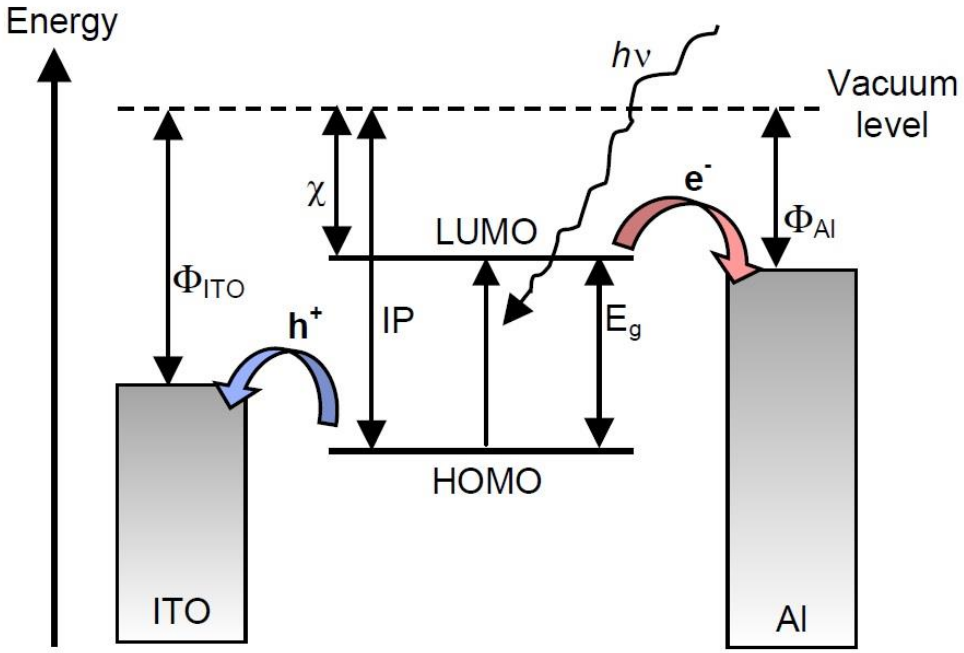

Figure 2.3: Energy levels and light harvesting [3]

A conduction band (CB) and a valence band (VB) is formed in the solid phase. This happens when the HOMO and LUMO of adjacent molecules interact with each other. Contact with electrodes changes the shape of the CB and VB and this change depends on the polymer conductance and the electrode connections. Under short circuit, the Fermi levels of the electrodes align (Fig. 2.5, B and C) leading to the shape change in CB and VB as mentioned above. The field in B changes linearly since it is an insulator while C is a p-type semiconductor. Charge carriers are generated under illumination and a Schottky junction is formed towards the high work-function electrodes as the holes flatten the bands in that direction since they are allowed to redistribute freely. This is due to the p-conduction properties. The depletion width is the curvature distance which is less than half the material thickness in C [3].

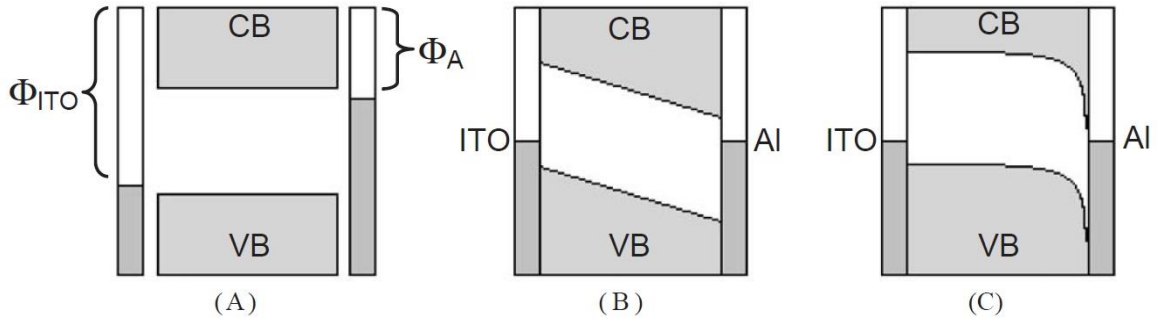

Figure 2.4: Relative energy levels of electrodes. Al is the low work-function electrode and ITO is the high work-function one. B is an insulator and C is a hole conducting polymer [3]

2.2 Comparison with conventional solar cells

The fundamental difference between most organic dye semiconductors and crystalline organic semiconductors is that the individual LUMOs and HOMOs form CB and VB throughout the material. Since the intermolecular forces in the in the organic dye semiconductors are too weak, the HOMOs and LUMOs don't have a strong enough interaction and the charge transport occurs by hopping between localized states unlike transport within a band in inorganic semiconductors. This leads to a lower charge carrier mobility and difficult charge separation in organic semiconductors due to the low dielectric constant. The electrons in an organic semiconductor are also bound to holes at room temperature. When the excitons are delocalized instead of localization on specific chain segments, they are known as polarons. The effective light harvest thickness of the organic semiconductors is also limited since the excitons formed in the middle of a thick layer are unable to reach the electrode interface and recombine instead. This is because the typical exciton diffusion distances are on the order of 10 nm [3].

2.3 I-V characteristics

Illumination shifts the dark I-V curve (Fig. 2.6) of a solar cell downwards. The amount of shift is known as the short-circuit current (I_{sc}). The V_{oc} or open circuit voltage between the two electrodes is around 0.5 – 1.5 V. Illumination of the cell in open circuit leads to its electrons flowing toward the low work-function electrode and the holes towards the high work-function electrode, which in turn leads to a charge build-up, the maximum value of which is the V_{oc}. I_{sc} is measured by illuminating the cell when the potential across it is zero, this also gives information about the efficiency of charge transport and also its separation. The maximum work of the cell is given as I_{max} V_{max} and the Fill Factor is calculated as I_{max} V_{max}/ V_{oc} I_{sc}. The number of electrons generated per photon absorbed is known as the quantum efficiency (QE). The Power Conversion Efficiency (PCE) is calculated as the power output divided by the power of incident light [3].

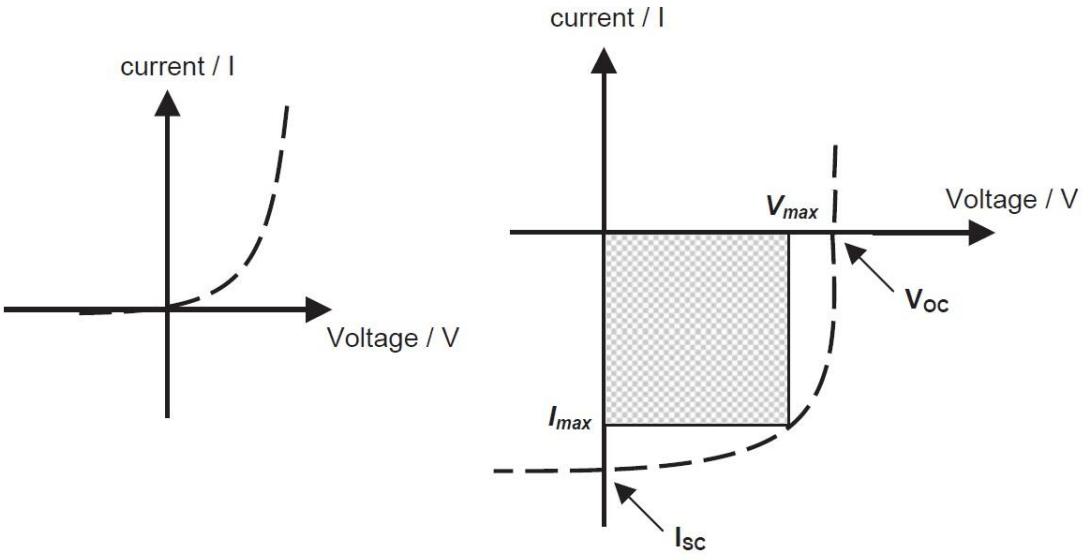

Figure 2.5: I-V curve of an organic PV cell under dark (left) and illuminated (right) conditions [3]

2.4 Conjugated polymer (CP) cells and Heterojunctions

PVK (poly(vinyl carbazole) was one of the first photoconducting polymers followed by other highly conducting polymers such as poly(sulphur nitride) and polyacetylene (PA). Earliest PA/ graphite cells were found to have a low open-circuit voltage of 0.3V and a quantum efficiency of 0.3%. Low efficiencies and low V_{oc}s in polythiophenes were later attributed to the formation of polarons which relax energetically in energy gap. This leads to a hugh spectral shift in the comparison between absorption and luminescence spectra. PPV and poly(alkyl-thiophenes) are the other widely investigated polymers for PV application [3].

Heterojunction implies a very simple and novel idea of utilizing materials that have different electron affinities and ionization potentials. This is done because excitons do not easily dissociate in most organic semiconductors. So, the material with larger electron affinity attracts electrons and the holes are pulled by the material with a lower ionization potential. For example, when an inorganic cell is sensitized using an organic dye in the respective spectral range, the LUMO of the dye is above the CB of the inorganic solar cell which leads to the transfer of electrons in the LUMO of the dye to CB of the inorganic material, thereby enhancing the conductivity. Similarly, in the case of a heterojunction PV device, if the LUMO of acceptor material is lower than that of the active material, the excited electron in LUMO of active material is relaxed into LUMO of acceptor material and from there, into the electrode. This provides a channel for electron flow, thereby reducing the recombination of excited electrons and holes. This phenomenon is depicted in Fig. 2.7. The separation at active layer/ acceptor interface is much more efficient than that at the acceptor/ electrode interface. Fullerene C_{60} molecules are one of the most used acceptors in heterojunctions. This is because of their excellent electron affinity and conductance properties [3].

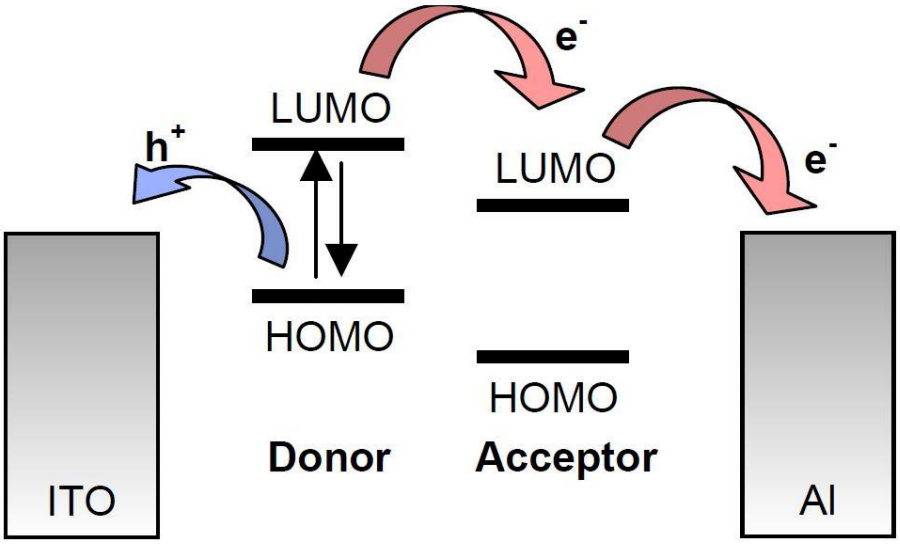

Figure 2.6: Exciton dissociation at the donor/ acceptor interface [3]

Control of interfaces in heterojunctions is of utmost importance, since the charge separation is affected by the effective donor-acceptor interface. But, with increasing interfacial layer thickness, the distance electron and holes need to travel to conduction layer also increase leading to recombination [3].

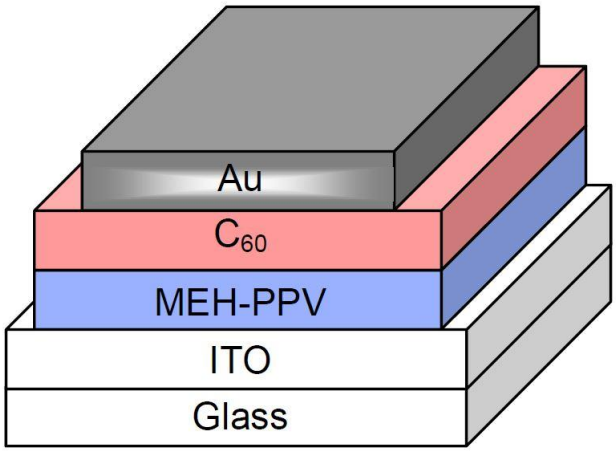

Figure 2.7: Two layer heterojunction cell with C_{60} as acceptor layer and MEH-PPV as the active/ donor layer [3]

2.5 Bulk Heterojunction

One of the big issues in heterojunctions is that, the diffusion lengths that electrons and holes can travel is on the order or 10 nm for effective exciton dissociation, hence the dissociation is most effective at the interface in these cells. But, for effective light harvesting, the layer should have a thickness greater than 100 nm so that it absorbs most of the light. Hence, in order to overcome this issue, the donor and acceptor materials are blended and this concept is known as bulk or dispersed heterojunction [3].

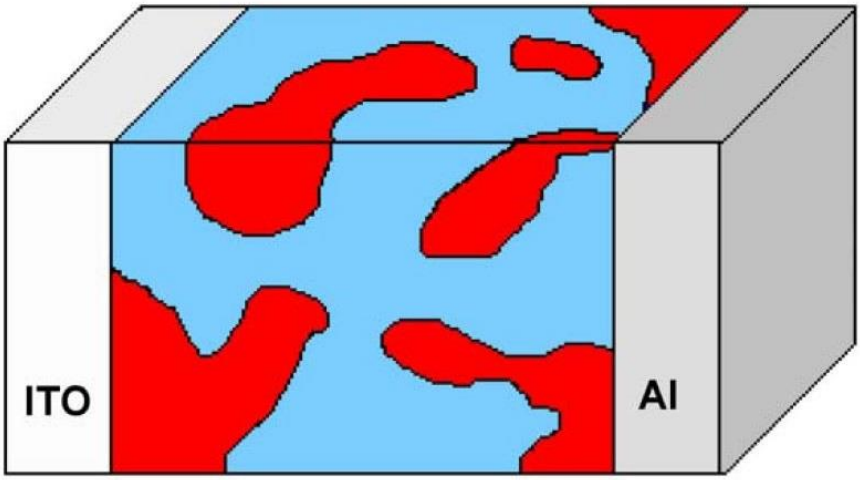

Figure 2.8: A Bulk heterojunction PV device [3]

However, solid state miscibility is an issue for these systems since miscibility of large extended conjugate systems is not good, especially for conjugated polymers. So it is necessary to avoid equilibrium, making necessary the use of spin casting with fast solvent evaporation. One issue with this approach was the low solubility of fullerenes in normal solvents, which was addressed by synthesis of C_{60} – derivatives like methano-functionalized fullerene derivatives bumping up

the fullerene content values to about 80%. P3HT (poly(3-hexylthiophene)/ methanofullerene bulk heterojunction were shown to have quantum efficiency values as high as 76% and the limitation was found to be due to the optical loss in the cell. The organic layer (dispersed) was found to contain an interpenetrating network of domains with typical sizes around 10 nm, thus being comparable to the diffusion length. These domains were found to be micro-phase separated blends. Also, a free path is required for holes and electrons to reach the respective electrodes without having to tunnel through the domains and hence, the network needs to be bicontinuous [3].

2.6 P3HT (Poly(3-hexylthiophene))

Alkylthiophene containing poly(heterocycles) have good chemical stability and solubility in common organic solvents besides having high conductivities and hence are an important class of materials among conjugate polymers. Among these, poly(3-hexylthiophene) is found to have good solubility, high mobility as well as decent film properties [4]. The chemical structure of P3HT is shown in Fig. 2.10 below.

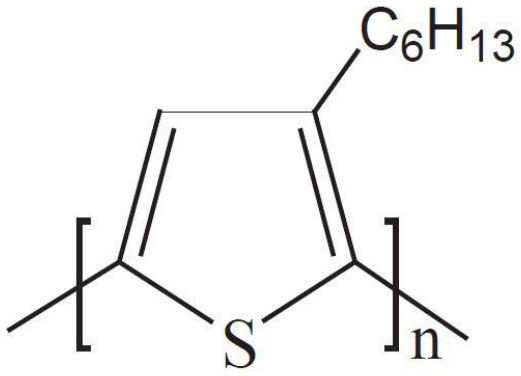

Figure 2.9: Chemical structure of P3HT [4]

Specific regions of the light spectrum received by Earth are lost due to atmospheric absorptions when light passes through it, according to the air mass that light passes. Just outside the Earth's atmosphere, the energy of light is 1366 Wm^{-2}. After the absorption loss, it becomes 1000 Wm^{-2}, at the Earth's surface (equator) according to AM 1. This AM is known as Air Mass, followed by a number which describing it. At Northern America latitudes, the absorption loss increases due to irradiance with sun being 45º above horizon and is known as AM 1.5. The knowledge of number of photons available for conversion into electrons at a particular wavelength of spectrum is important. Harvesting energy at longer wavelength is desirable, since it means more no. of charges are excited, hence higher value of J_{sc}, but the energy of charges excited at the wavelengths is also lower and hence limits the V_{oc}. Therefore, an optimum balance in the band-gap value is desirable [5]. Fig. 2.11 shows the sun spectrum.

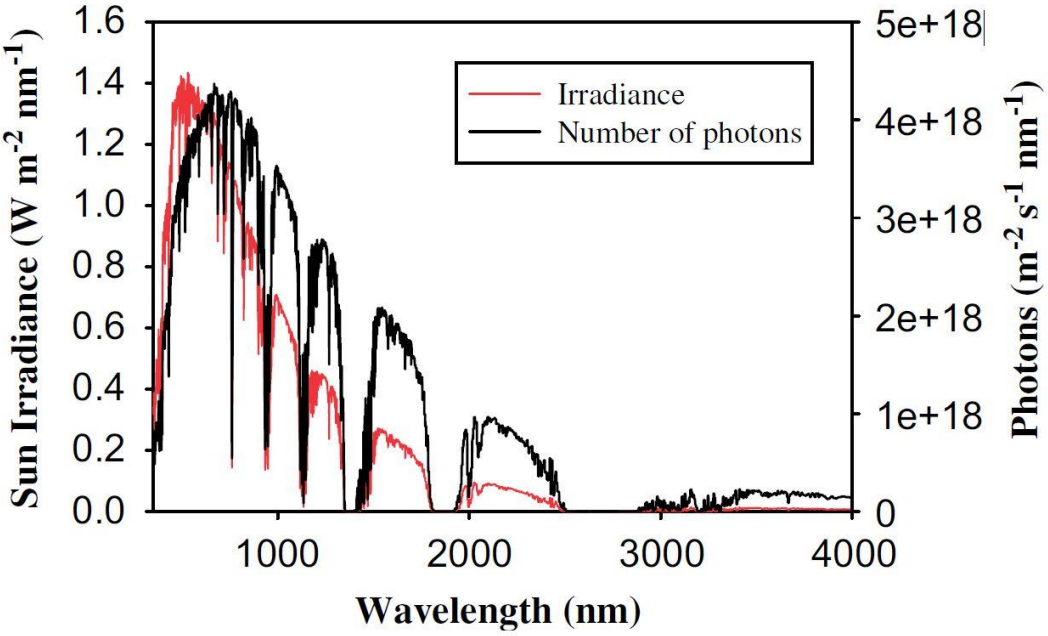

Figure 2.10: Sun irradiance and no. of photons as a function of wavelength [5]

Based on the above consideration, P3HT has a band-gap of 1.9 eV (650nm) and hence can harvest 22.4% of the incident photons leading to a max current density of 14.3 mA cm^{-2}. Hence, lower the band-gap, higher the no. of available photons for conversion. Device morphology, carrier mobility and lifetime also dictate the maximum current density that can be obtained. Reflection, multiple passage, scattering, interference should also be taken into account [5]. Table 2.1 below denotes these values for different wavelengths.

Table 2.1: Max current density available for a particular wavelength [5]

Wavelength	Max. % harvested (280 nm →)	Current density ($mA\,cm^{-2}$)
500	8.0	5.1
600	17.3	11.1
650	22.4	14.3
700	27.6	17.6
750	35.6	20.8
800	37.3	23.8
900	46.7	29.8
1000	53.0	33.9
1250	68.7	43.9
1500	75.0	47.9

Different alkyl groups have been experimented on in order to improve the solubility of polythiophenes. Owing to the polymerization processing through 2, 5 positions, there is the added possibility of region-regularity in these polymers where, region-regularity is desirable. This regio-regular behavior arises from the possibility of the polymerization reaction moving forward in a head to tail, head to head or tail to tail fashions. Since, regio-regularity dictates the effective conjugation length of the polymer; it also dictates the molecular weight. When the

molecular weight and effective conjugation length (de-localisation of Π electrons on the backbone chain or structure) increase, the band-gap of the material narrows down and hence, it has a higher value of the maximum wavelength that can be absorbed. Regio-regularity also dictates packing of the polymer and in case of P3HT, forms an inverted comb like structure of layers. P3HT also displays solvatochromism, meaning it has different absorption spectrum in solution and thin film forms. This is because, when in solution, the side chain interacts with the solvent molecules and leads to enhanced twisting of the side chain, reducing effective conjugation length. So, the band-gap increases and hence the absorption spectrum is also different as can be seen in Fig. 2.12 below. Regio-regularity also influences the morphology of bulk heterojunction [5].

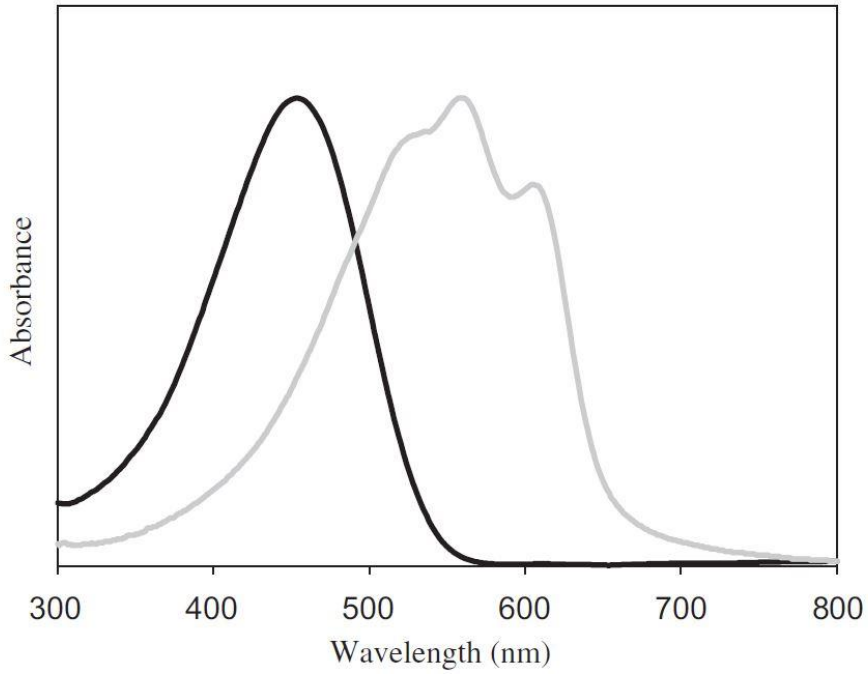

Figure 2.11: orption spectra of P3HT in solution (Black) and in solid film (Grey) [5]

Bulk heterojunction devices of P3HT: PCBM are interplay of highly region-regular, high molecular weight material and a low region-regularity, low molecular weight material. The PCBM plays an important role as glue in the interface between PCBM nano-crystals and P3HT domains. Lifetime data analysis of these materials has been hardly touched by research groups. PCBM content influences the hole and electron mobility in these devices. An increase in the PCBM content increases the electron mobility while slightly reducing the hole mobility. In order to achieve high IPCE, a 240 nm thick layer of active material is needed since the mean drift length of charge carriers much exceeds the active layer thickness. So, increase in thickness leads to increase in I_{sc} due to higher amount of light being absorbed [5].

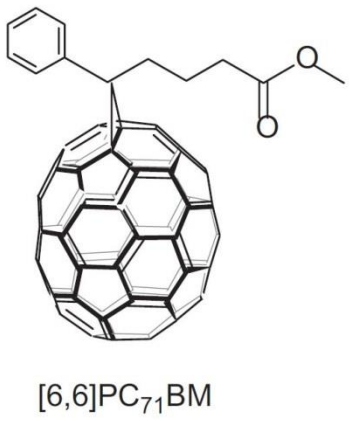

Figure 2.12: Structure of PC71BM electron acceptor [5]

2.7 Inverted Device Structure

Conventional hole transport layer (PEDOT:PSS) and low work-function metal cathode materials are corrosive and hygroscopic and hence detrimental to device lifetime. The inverted devices are made using ITO modified by n-type metal oxides or carbonates and demonstrate superior long

term ambient stability. Top electrodes are air stable metals hence provide natural encapsulation along with the added benefits of vertical phase separation and concentration gradient in the active layer. Inverted structures have a higher J_{sc} than the conventional ones and this is due to the combination of increases optical absorption, as well as reduced bimolecular recombination and this observation of difference in J_{sc} is independent of the active layer thickness. The inverted devices show a decrease in the reflectance compared to the conventional structures, which explains the increase in optical absorption over a wide range of spectra 9400 -800 nm). Also, the redistribution of electric field intensity of the incident photons inside the active layer in these inverted structures also contributes to the optical absorption enhancement [6].

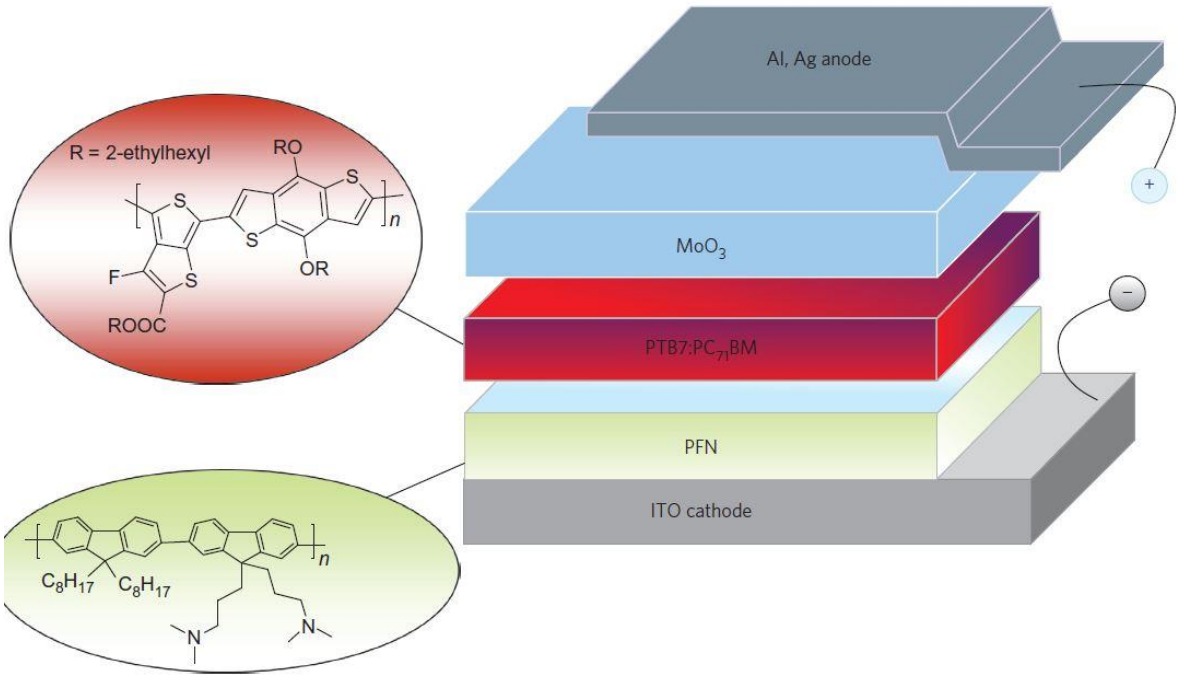

Figure 2.13: Schematic of inverted structure device [6]

Both devices have a very high Fill Factor value (70%) and also show that their dependence on incident light is comparable hence proving that any difference in recombination loss in the device can be neglected. PFN devices (PFN used as electron transfer layer) show better light harvesting compared to ZnO devices. Inverted structure provides ohmic contact for photo-generated charge carries (Fig. 2.15 below) in addition to providing optimum amount of photon harvest from the sun's spectrum [6].

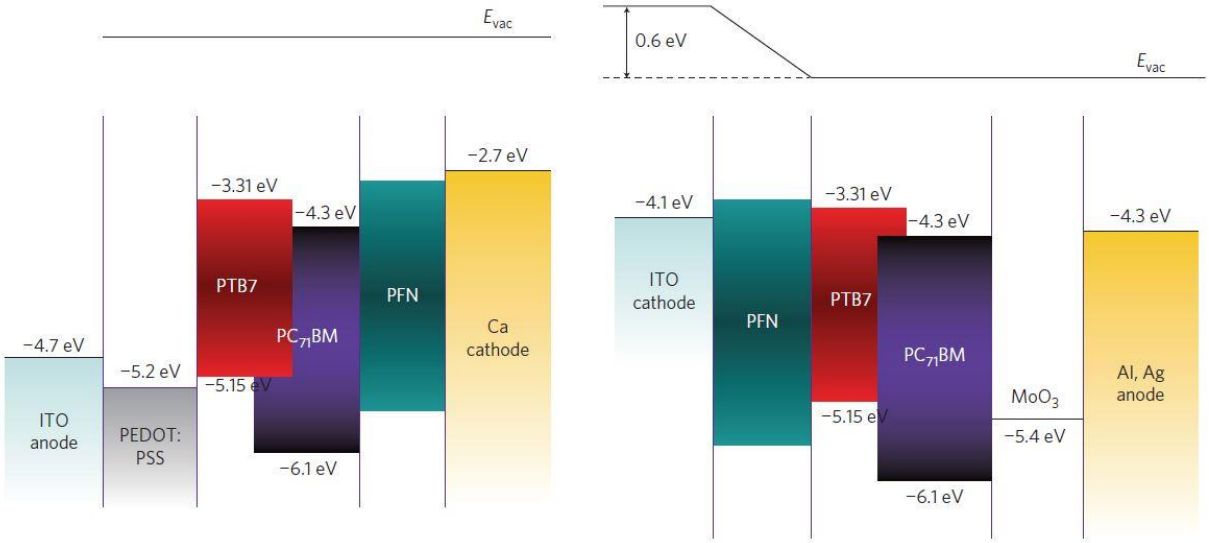

Figure 2.14: Schematic energy levels of conventional (left) and inverted (right) structures under flat-band conditions [6]

3 Experimental Methods

3.1 Substrate Cleaning

ITO coated glass substrates having an area of 1 cm^2 were used for this study. The first step in the cleaning operation was removal of Photo-resist. This was done using Acetone. The substrates were immersed in a cylindrical container of Acetone for about 3 - 5 seconds. The acetone was recycled back into the container. Next, Isopropyl Alcohol (IPA) was used. The substrates were immersed in a cylindrical container of IPA and subjected to Sonic Cad for 15 minutes. After sonic cad treatment, the IPA was recycled. Next, detergent + de-ionized water mix was used, followed by sonic cad treatment for 15 minutes. The sonic cad treatment was repeated again using de-ionized water for 15 minutes, since this treatment removes dust, oil, etc. Next, the substrates are subjected to sonic cad treatment again while immersed in acetone for 15 minutes followed by the last cleaning step, which was another sonic cad treatment for 15 minutes using new IPA solution. The IPA was recycled and the substrates are put inside an oven to dry for an hour at least. The temperature used was 100 ºC. Fig. 3.1 below denotes the detailed flow chart of the cleaning steps involved.

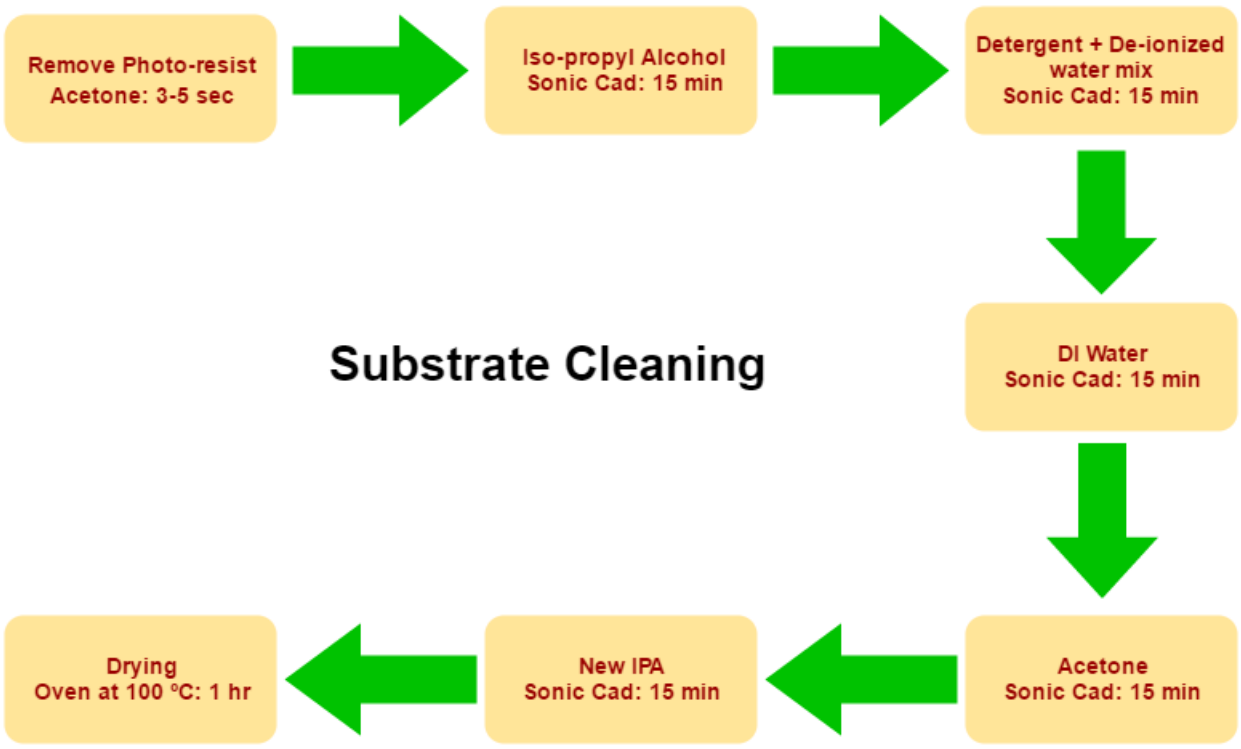

Figure 3.1: Schematic flow diagram showing substrate cleaning steps

3.2 Bulk Heterojunction Solution (P3HT:$PC_{71}BM$)

The active layer of the device is a polymer mix of P3HT and $PC_{71}BM$ in 1:1 ratio. The solvent used was DCB (Dichlorobenzene) and the solution was 2 wt. % strong. The solution was allowed to stir overnight (minimum 8 hours) using a magnetic stirrer. No heat was required. The solution was always filtered before building the devices. Table 3.1 shows the various solvents and ratios experimented for this bulk heterojunction polymer mix.

Table 3.1: Photovoltaic responses obtained for P3HT [5]

M_w (M_w/M_n)	P3HT/ PCBM	Solvent	Area (cm^2)	Annealing temperature (°C)	I_{SC} ($mA\,cm^{-2}$)	V_{OC} (V)	FF (%)	η (%)	IPCE/λ (%, nm)	Notes	Refs.
RM:	—	DCB	0.05–0.08	75 (4 min)[a]	8.5	0.55	60	3.5	70/500	$800\,Wm^{-2}$	[105]
RM: 30000	1:1	DCB	0.11	110 (10 min)	10.6	0.60	67.4	4.4	63/500	Ca/Al	[106]
RM: 87000	1:1	—	—	155 (2–3 min)	10.1	0.86	61	5.2	—	$80\,mWcm^{-2}$	[10]
RM:	1:0.8	CB	0.148	150 (30 min)	9.5	0.63	68	5.0	60/500[b]		[11]
RM:	1:2	THN	0.025–0.04	120 (10 min) 100 (5 min)	11.8	0.54	56	3.6	—		[107]
RM: 30000	1:1	DCB	0.105	110 (10 min)	8.94	0.6	61.9	3.33	63/500	ITO/MoO_3 (5 mm), Ca/Al	[108]
RM:	1:1	$CHCl_3$		130 (20 s)	6.35	0.60	63	2.39	62/500		[109]
RM:	1:2	CB	0.02	75 (4 min)	15.2	0.54	37[c]	—	15/340 65/540	Xe-lamp	[110]
AD: 36000 (1.9)	1:2 PCBG	DCB	—	140 (4 min)	5.2	0.53	62	>2	—		[111]
AD:	1:2	Toluene	0.09	96 (1 min)	8.16	0.58	45.5	2.15	8/475	PET substrate	[112]
MK: 44000–28000	1:1	CB	0.045	50 (30 min), 140 (4 min)[d]	0.85	0.6	—	1.14	35/500		[113]
—	35:1 (C_{60})	CN/BFEE (1:2)	0.09	No annealing	0.3	0.81	38	0.3	—	Electrochemical polymerisation,[e] Ca/Ag	[114]
—	1:3	—	0.04	—	8.7	0.58	55	2.8	76/550	$50\,mW\,cm^{-2}$, Ca/ Al	[115]
100000 (2.14)	1:1	DCB	1.0	120 (60 min)	7.2[f]	0.615	61	2.7	56/500		[116]
19000	1:1	CB	4	80 (30 min)	9.9	0.60	41	2.41	60/550	Mg/Al	[117]
52100 (2.19)	1:1	CB	0.06–0.08	120 (4 min)[g]	5.64	0.58	62	2.09	30/500	$97\,mWcm^{-2}$	[118]
19000 (1.35)	1:1	Xylene	0.04	—	10	0.6	55	3.2	55/550	Ca/Ag	[39]

3.3 Device Fabrication

The substrates are blow dried with N_2 after every step in the fabrication process. The first step was to deposit the electron transport layer on the cleaned ITO coated glass substrates, which in this case is Zinc Oxide (ZnO). Approximately 13 µL of ZnO solution was taken in a pipette and dropped on the ITO side of the substrate, followed by spin coating at 2500 rpm for 30 sec. Next, the ZnO layer was annealed on a hotplate at 150 ºC for 15 minutes followed by cooling to ambient temperature. Next, the active layer is deposited on the annealed ZnO layer. The active or light absorbing layer solution made earlier is deposited onto the substrate using a glass pipette and spread evenly on the surface. Next, the spin coating is done in two stages; the first stage is 800 rpm for 30 sec followed by 2000 rpm for 1 sec in order to get rid of the access solution. After spin coating, the devices are covered using a petri dish for slow growth mechanism to occur. The color of the substrates turns to dark red from light red, signaling the end of slow growth process. This basically means that the band-gap shortens, since the color tunes towards longer wavelength, hence signifying longer effective conjugation lengths in the thin film. The

active layer is then annealed at 130 ºC for 10 minutes. The final steps are the deposition of hole transport layer and the metal contact or electrode. This was done using thermal evaporation or physical vapor deposition (PVD). The deposited layer thickness is 20 nm for MoO_3 and 150 nm for Al. Deposition is done under a vacuum pressure of $5 * 10^{-6}$ Torr. For MoO_3 deposition, 0.05 nm/ sec rate is used and for Al deposition, 0.15 nm/sec rate is used. After coating MoO_3, the substrates are removed and thin lines are scratched on the border in order to reveal the ITO, since the low and high work-function electrode contacts are on the same side of the device. Next, shadow masks are used to deposit Al fingers as the metal contact or electrode on the device. Fig. 3.2 below shows a detailed flowchart of the device fabrication process.

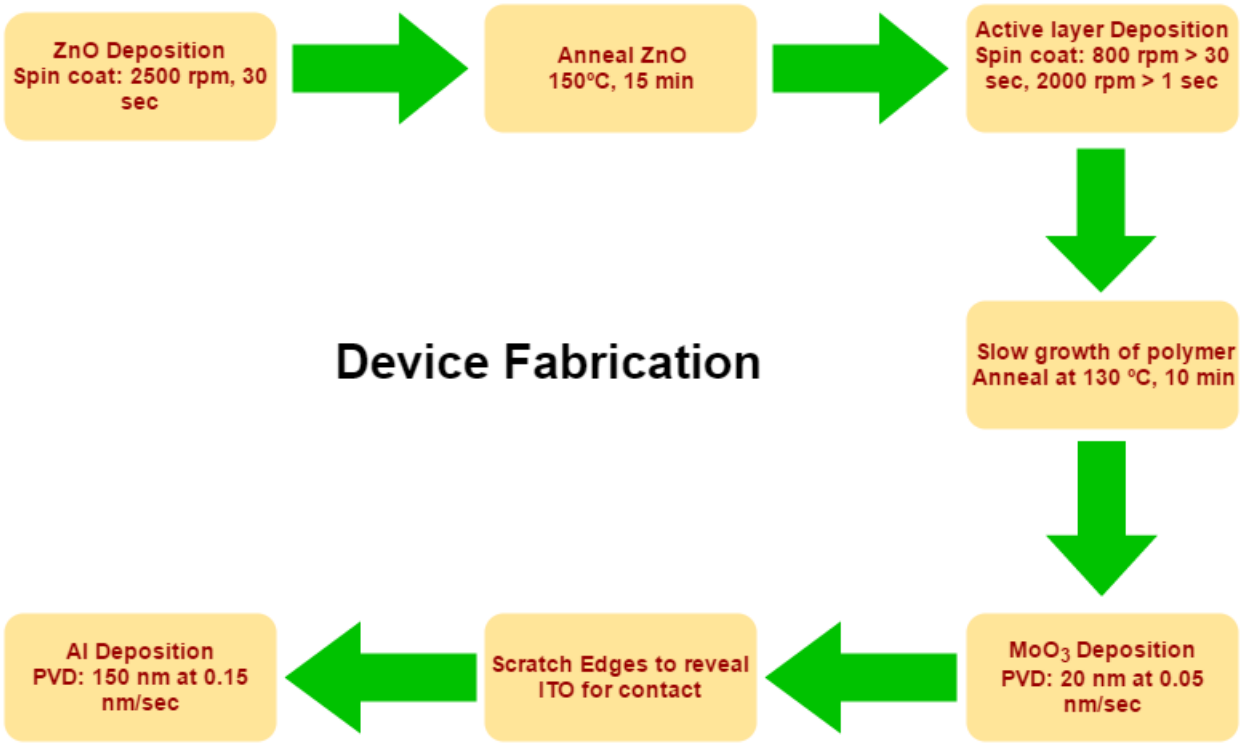

Figure 3.2: Schematic process flow of device fabrication steps

3.4 Ozone Exposure

The ozone exposure experiment was conducted in two parts. In the first part, the effect of ozone oxidation on the active polymer layer was investigated. Hence, after coating and annealing the active layer, the devices were exposed to ozone environment at different time intervals at ozone concentration of 300 ppb (Table 4.1), 600 ppb (Table 4.2) and ambient exposure of 70 ppb (Table 4.3). After exposure, these devices were completed by coating the anodes using thermal evaporation (MoO_3 as the hole transport layer and Al as the metal contact). Next, these devices were subjected to J-V measurement for investigating the decay in efficiency and fill factor with respect to the strength and length of exposure. The process flow of this part of the experiment is shown schematically in Fig. 3.3.

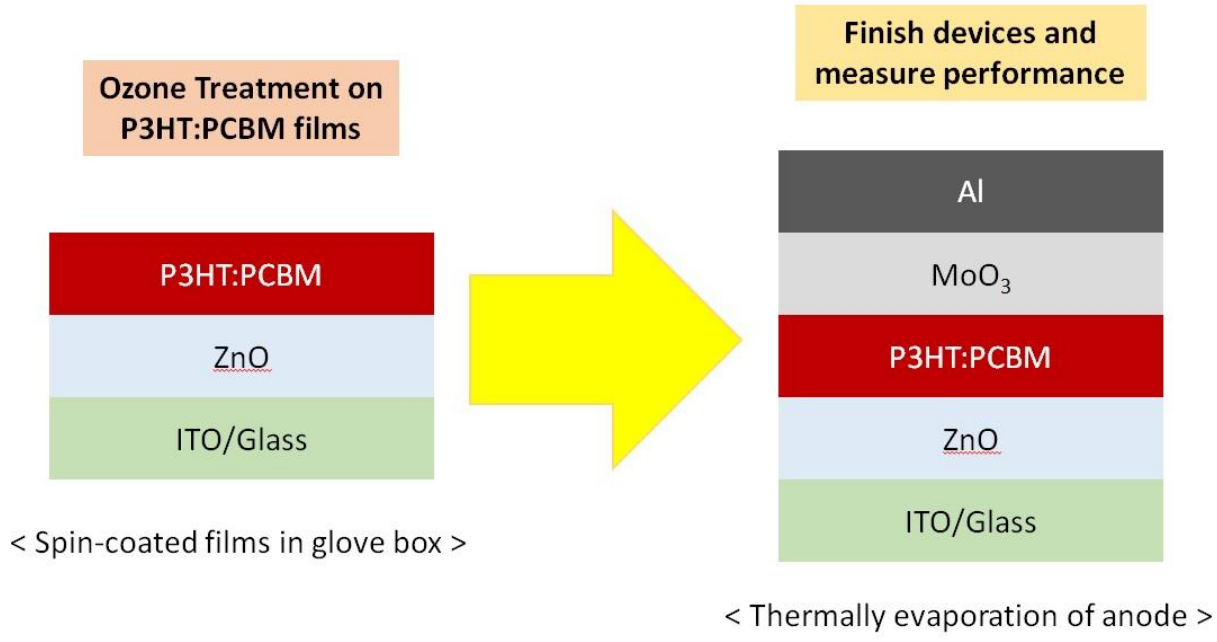

Figure 3.3: Schematic process flow for Ozone Exposure Part 1

In the second part of the experiment, the devices are completed, including coating of anode materials, viz., MoO_3 as the hole transport layer and Al as the metal contact using thermal evaporation. Later, these completed devices were exposed to ozone environment having a concentration of 400 ppb followed by J-V measurement as detailed in the earlier part for investigating efficiency and fill factor decay. The results are displayed in Table 4.4 and Fig. 3.4 shows a schematic diagram of the process flow.

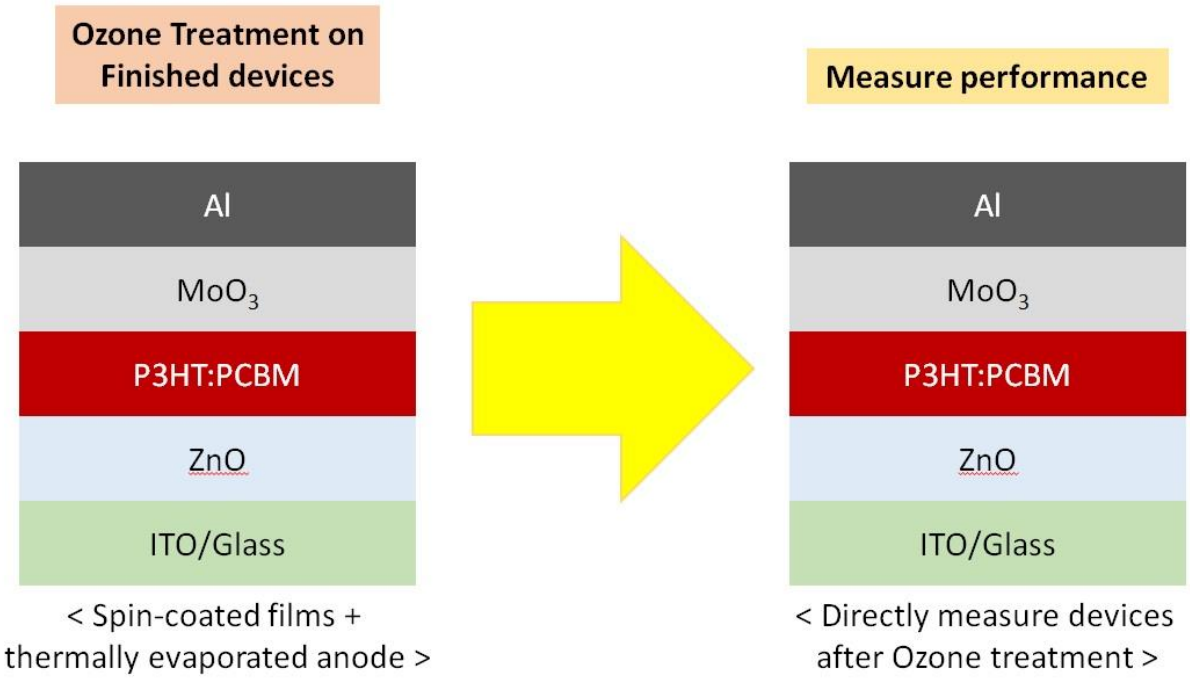

Figure 3.4: Schematic process flow for Ozone Exposure Part 2

3.5 Efficiency and Fill Factor measurement

The devices were subjected to J-V measurement under AM 1.5 condition (1 sun or power density of 100 W/m^2). First, the light source allowed to warm up for 10 minutes and was calibrated to operate at 1 sun condition using a standard photo-diode of known current co-efficient. Then the devices were exposed to light and J-V sweep was done for each of the 4 Al finger contacts spread across the device which generated the J-V curves. Different fingers are used in order to check uniformity of the device. Power conversion efficiency (PCE) and Fill Factor (FF) were calculated from the data for different ozone concentration and lengths of exposure.

3.6 Fourier Transform Infrared Spectroscopy (FTIR)

The first step to understand the degradation mechanism would be to analyze the role and effect of ozone oxidation on the polymer materials. In order to do this, FTIR measurements were employed to study the change in the absorption or transmission spectrum of these materials, especially in the C-O bond absorption region. All materials absorb light of a particular wavelength corresponding to their structure, i.e. the shape and type of molecules present, their vibration, etc. Hence, the absorption spectrum from the unaffected material was obtained and compared with the exposed material to note the change in absorption peaks which gives critical information about the change in skeletal structure as well as functional groups of the polymer in question due to the effect of ozone oxidation. Transmission spectrum was measured for polymer materials coated on Glass substrate as well as Silicon substrate and exposed to ozone concentration of 600 ppb for varied duration. Absorption spectrum (FTIR-ATR) was measured for polymer materials coated on glass substrate and exposed to different lengths of time under ozone concentration of 600 ppb.

4 Results and Discussion

4.1 Device Structure and Properties

The fabricated device structure (vertical) is as shown in Fig. 4.1 below with ITO as the low work-function contact, ZnO as the electron transport layer, P3HT:$PC_{71}BM$ as the active layer of the Bulk heterojunction cell, MoO_3 as the hole transport layer followed by Al as the high work-function contact. This structure is known as the inverted device structure.

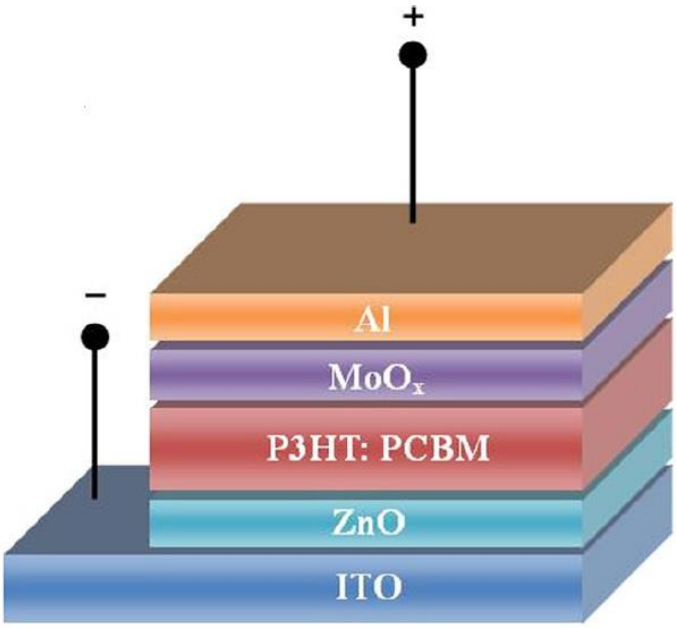

Figure 4.1: Schematic view of structure of inverted solar cell [7]

The flat band diagram of the device is shown in Fig. 4.2 followed by the typical J-V curve (Fig. 4.3) obtained from such unexposed (ozone) devices.

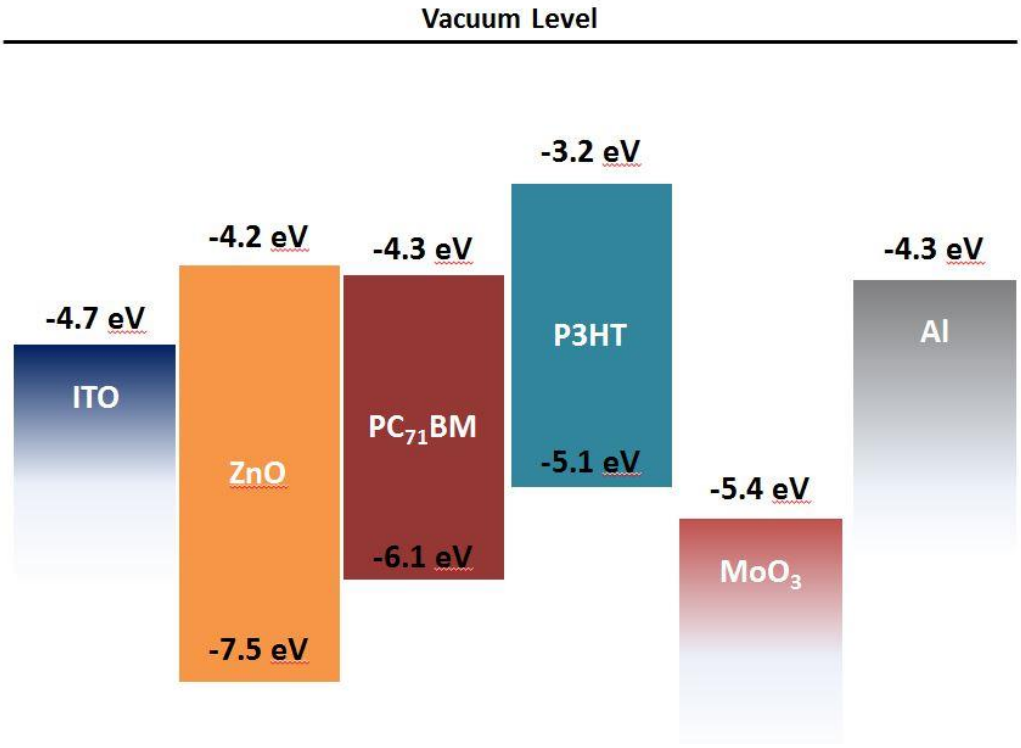

Figure 4.2: Schematic energy levels of the devices fabricated for this study [8, 15 - 16]

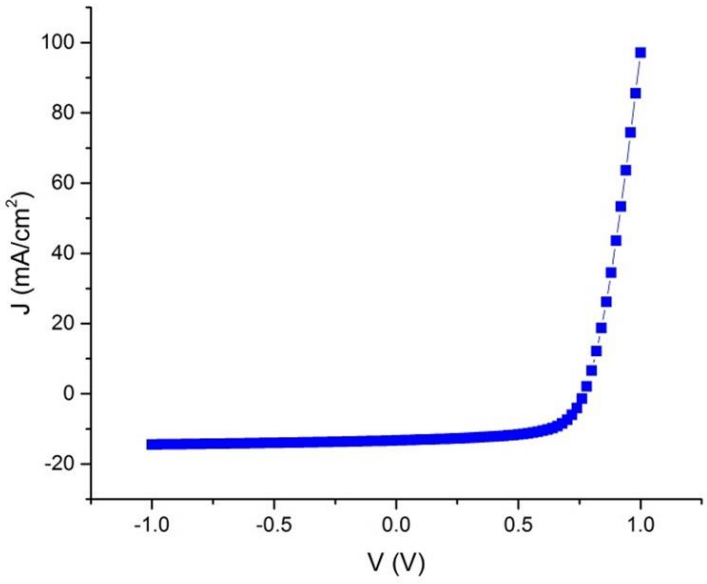

Figure 4.3: Typical J-V curve for unexposed P3HT:$PC_{71}BM$ device

4.2 Ozone Exposure Results

4.2.1 Part I: Only Polymer films exposed to Ozone

For the first part of the experiment, where only the active layer was exposed to ozone (without the coated anodes), Table 4.1 below shows the drop in PCE with time for the devices exposed to 300 ppb (±10%) ozone concentration.

Table 4.1: Power conversion efficiency (PCE) and Fill Factor drop in polymer films exposed to 300 ppb (±10%) of ozone concentration from 0 min to 12 hours (720 minutes)

Exposure Time (hours)	Voc (V)	Jsc (mA/cm^2)	PCE (%)	Fill Factor (%)
0	0.593	11.74	4.05	58.16
0.5	0.552	10.50	3.37	58.15
1	0.533	9.72	2.86	55.27
3	0.469	9.30	1.35	30.96
6	0.423	4.72	0.34	17.11
9	0.344	0.83	0.05	16.24
12	0.020	0.03	0.00	0.00

As can be seen from the Table 4.1 above, the devices with only polymer films exposed to ozone at 300 ppb (±10%) concentration, they decay to 0% efficiency (PCE) and 0% Fill Factor in 12

hours. Fig 4.4 below shows the exponential decay curves plotted between PCE and exposure based on the data observed in Table 4.1.

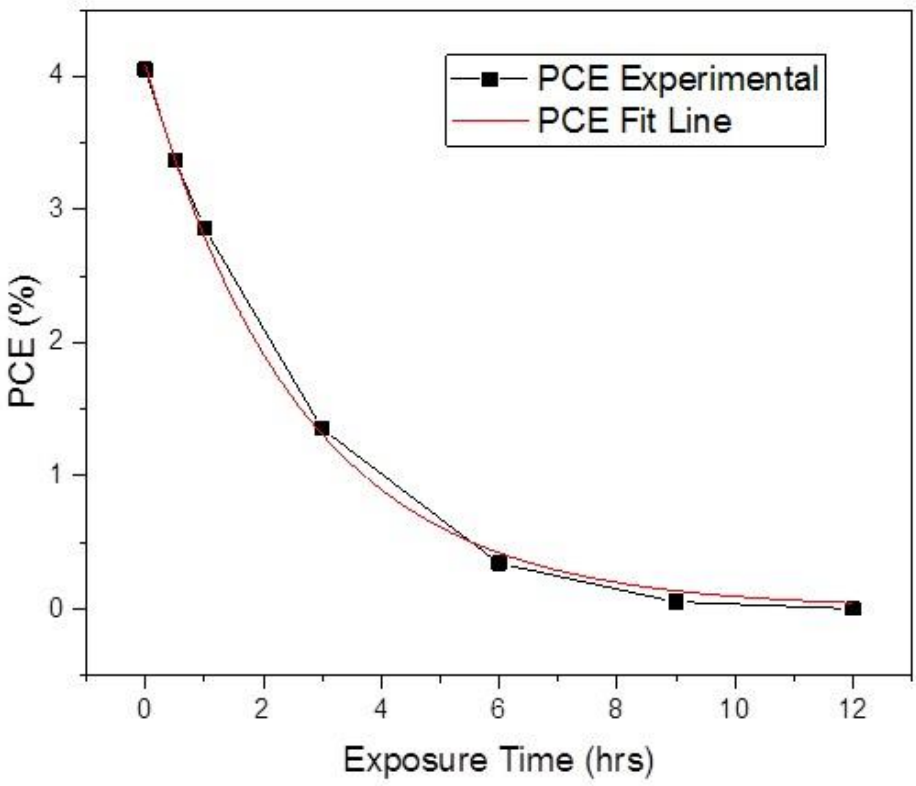

Figure 4.4: PCE vs. Exposure time for polymer films exposed to 300 ppb (±10%) of ozone concentration from 0 min to 12 hours (720 minutes)

Time constant for the exponential decay was found using curve fitting with the following equation:

$$PCE = PCE_{(0)} \times exp(-\frac{t}{\tau})$$

The time constant for the above Fig 4.4 was found to be $\tau = 2.6 \pm 0.1$ hours.

Table 4.2: Power conversion efficiency (PCE) and Fill Factor drop in polymer films exposed to 600 ppb (±10%) of ozone concentration from 0 min to 6 hours (360 minutes)

Exposure Time (hrs)	Voc (V)	Jsc (mA/cm^2)	PCE (%)	Fill Factor (%)
0	0.538	12.53	3.42	50.79
0.25	0.490	9.51	2.29	49.20
0.5	0.508	9.68	2.47	50.23
1	0.480	8.85	1.90	44.64
1.5	0.512	8.55	1.28	29.19
3	0.447	2.23	0.15	15.09
4.5	0.415	1.18	0.08	15.70
6	0.450	0.75	0.05	13.95

In this case, it is observed that the devices decay to 0% efficiency in about 6 hours, since the ozone concentration was doubled to 600 ppb (±10%), establishing an inverse linear relationship between the decay rate and ozone exposure at high concentrations. Fig 4.5 below shows the exponential decay curves plotted between PCE and exposure based on the data observed in Table 4.2.

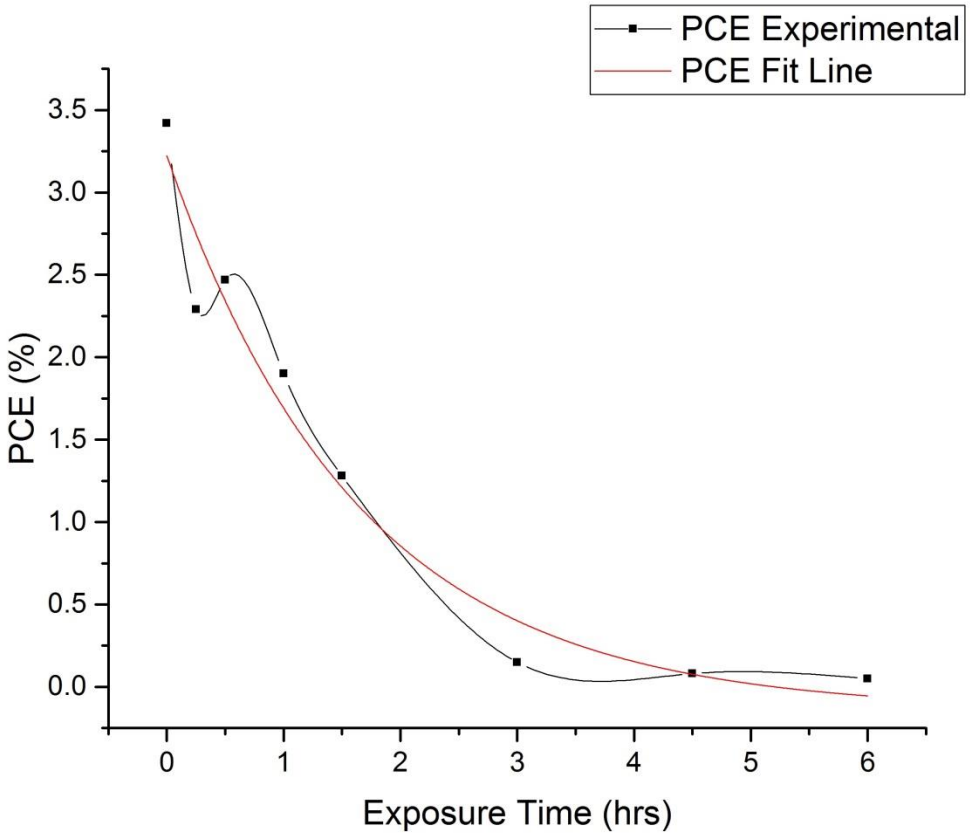

Figure 4.5: PCE vs. Exposure time for polymer films exposed to 600 ppb (±10%) of ozone concentration from 0 min to 6 hours (360 minutes)

The time constant for the above Fig 4.5 was found to be $\tau = 1.6 \pm 0.4$ hours using curve fitting with the above mentioned equation.

Table 4.3: Power conversion efficiency (PCE) and Fill Factor drop in polymer films exposed to 70 ppb (±15%) of ozone concentration (ambient) upto 28 hours

Exposure Time (hrs)	Voc (V)	Jsc (mA/cm^2)	PCE (%)	Fill Factor (%)
2.1	0.551	10.13	3.14	56.37
6.5	0.555	9.6	2.87	53.98
10.8	0.561	8.13	0.95	20.71
15.1	0.547	3.48	0.23	12.32
28.1	0.509	0.3	0.02	11.09
42.8	0.452	0.03	0	11.93
55.8	0.392	0.01	0	13.36

The Table 4.3 above shows the decay in devices exposed to ambient ozone concentration of 70 ppb (±15%) and it can be observed that the devices decay to 0% efficiency in about 28 hours, which is much faster than expected and also proves that oxidation effect of ozone on OPV materials also exists at ambient conditions. Fig 4.6 below shows the exponential decay curves plotted between PCE and exposure based on the data observed in Table 4.3.

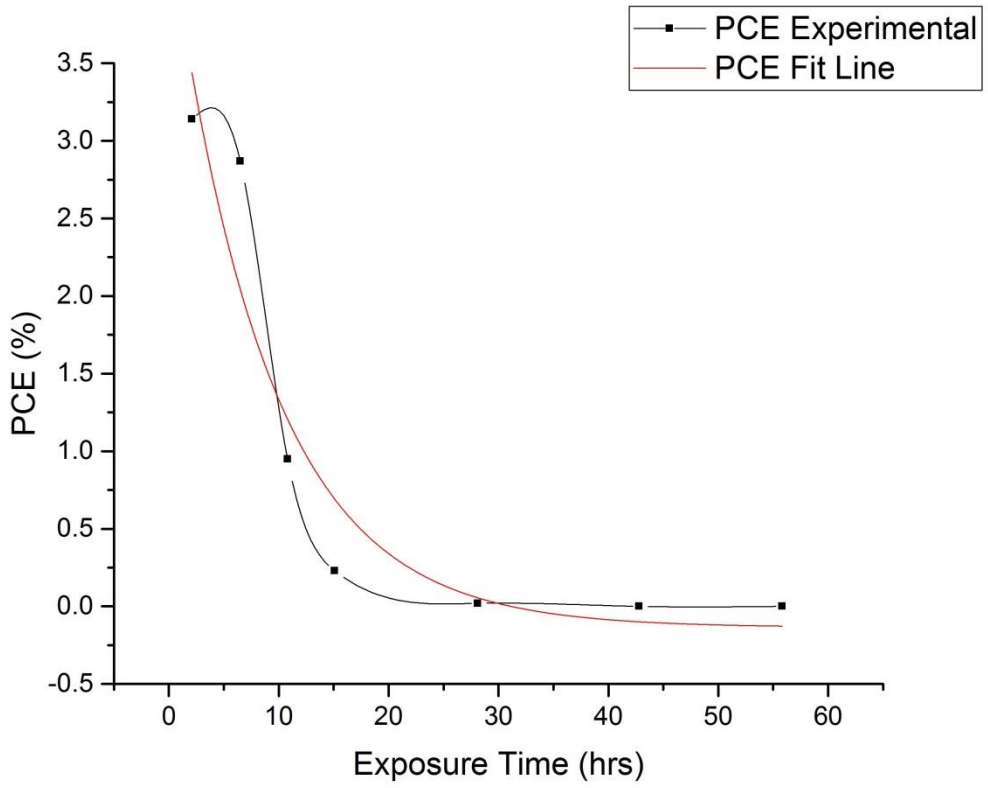

Figure 4.6: PCE vs. Exposure time for polymer films exposed to 70 ppb (±15%) of ozone concentration upto 28 hours

The time constant for the above Fig 4.6 was found to be $\tau = 8.9 \pm 3.3$ hours using curve fitting with the above mentioned equation.

4.2.2 Part II: Complete devices exposed to Ozone

The completed devices (with thermally evaporated anodes) were exposed to ozone environment having a concentration of 400 ppb followed by J-V measurement as detailed in the earlier part for investigating efficiency and fill factor decay. The results are displayed in Table 4.4 below.

Table 4.4: Power conversion efficiency (PCE) and Fill Factor of complete devices, exposed to ozone concentration of 400 ppb after coating of anodes (MoO_3 and Al)

Exposure Time (hrs)	Voc (V)	Jsc (mA/cm^2)	PCE (%)	Fill Factor (%)
2.1	0.611	10.68	4.13	63.33
6.5	0.597	11.36	4.08	60.22
10.8	0.595	12.48	4.41	59.3
15.1	0.598	11.44	4.14	60.52
28.1	0.596	11.65	4.19	60.42
42.8	0.604	10.7	4.02	62.18

The Table 4.4 above shows that the complete devices, with coated anodes have superior resistance to ozone oxidation since even after 42.8 hours of exposure to ozone concentration of 400 ppb, the devices show 4.16% efficiency with a standard deviation of 0.12%, which is a decent value for this polymer. Hence, the effect of ozone oxidation on the polymer films is considerably higher than on the anode materials. The anodes, viz. MoO_3 and Al, impart significant robustness to the devices against ozone oxidation.

4.3 FTIR Results

FTIR measurements were carried out on glass substrate first and then polymers coated on glass substrates exposed to an ozone concentration of 600 ppb in the transmission mode first. The idea was to compare the transmittance spectrum of the exposed samples with the unexposed samples and note out the differences as a starting point to understanding the degradation mechanism of ozone oxidation. But, as can be seen in the Fig 4.7 below, glass absorbs all infrared light less than 2000 cm^{-1} wavenumber. Hence, we cannot observe the changes in the skeletal structure of the polymer using this mode of measurement.

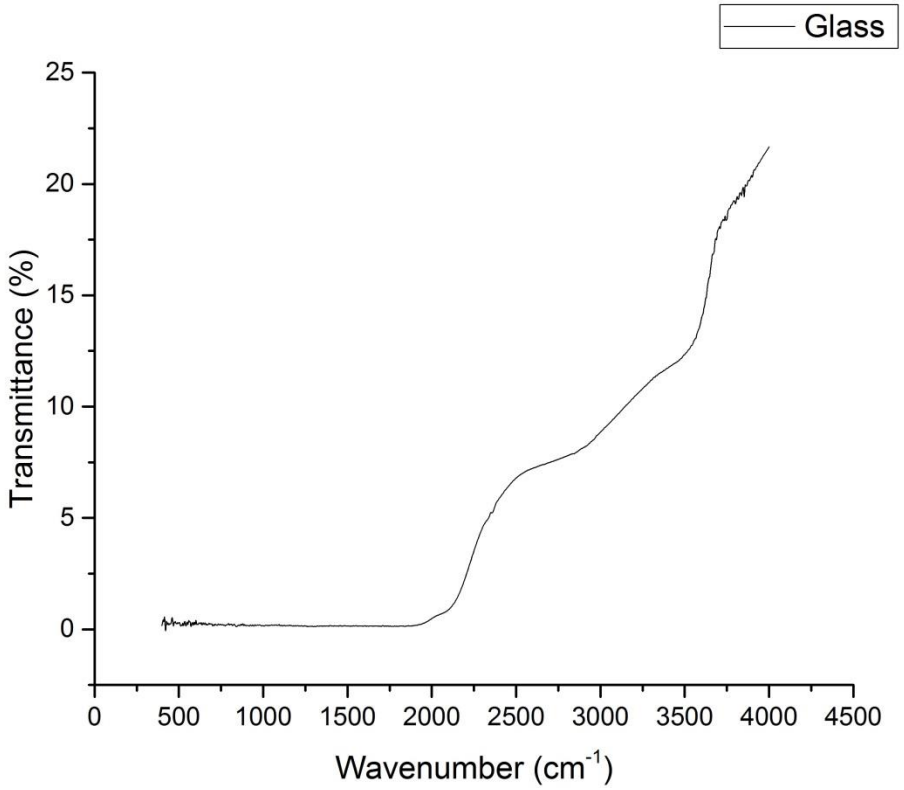

Figure 4.7: FTIR Transmission spectrum for Glass substrate only

Hence, absorption spectrum was measured next using FTIR-ATR (Attenuated Total Reflection). Typically, this method gives a comparatively weaker signal. Fig. 4.8 below shows the absorbance spectrum for polymer material coated on glass substrate and unexposed to ozone.

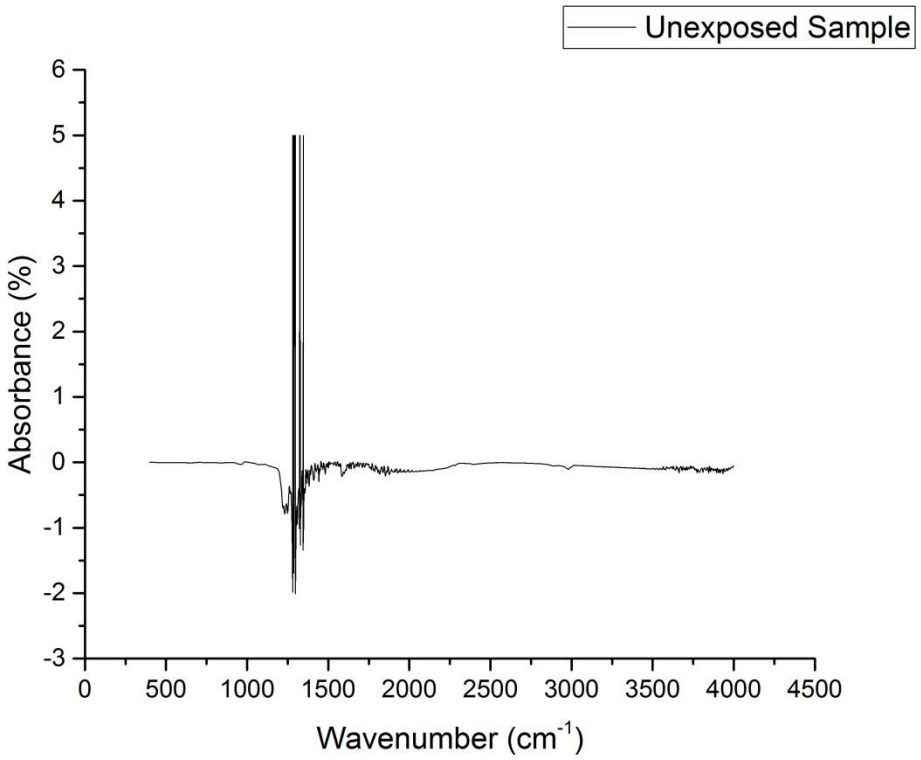

Figure 4.8: FTIR-ATR absorbance spectrum for polymer material coated on glass substrate

As can be seen above, the spectrum obtained is very noisy since it shows negative absorbance as well. This observation is reinforced in Fig. 4.10, where the absorbance spectrum from polymer sample exposed to ozone concentration of 600 ppb for 15 min is measured against the spectrum obtained from unexposed sample (this sample is treated as the background instead of atmosphere) so as to note the differences in absorption peaks. But, the spectrum obtained contains too much noise to discern any meaningful data from it.

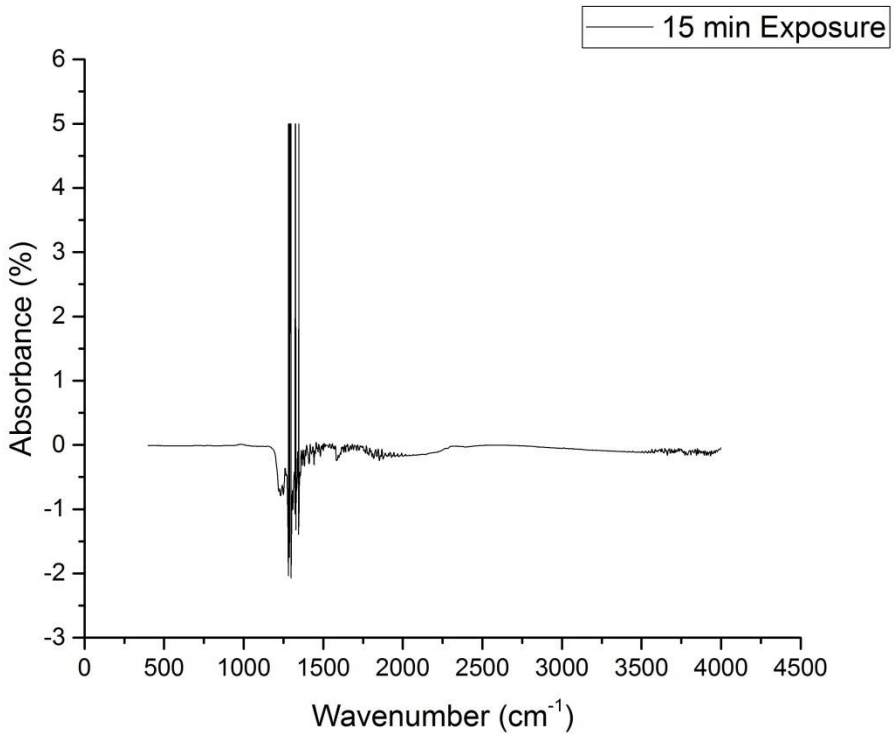

Figure 4.9: FTIR-ATR absorbance spectrum for polymer material coated on glass substrate and exposed to ozone concentration of 600 ppb (±10%) for 15 min

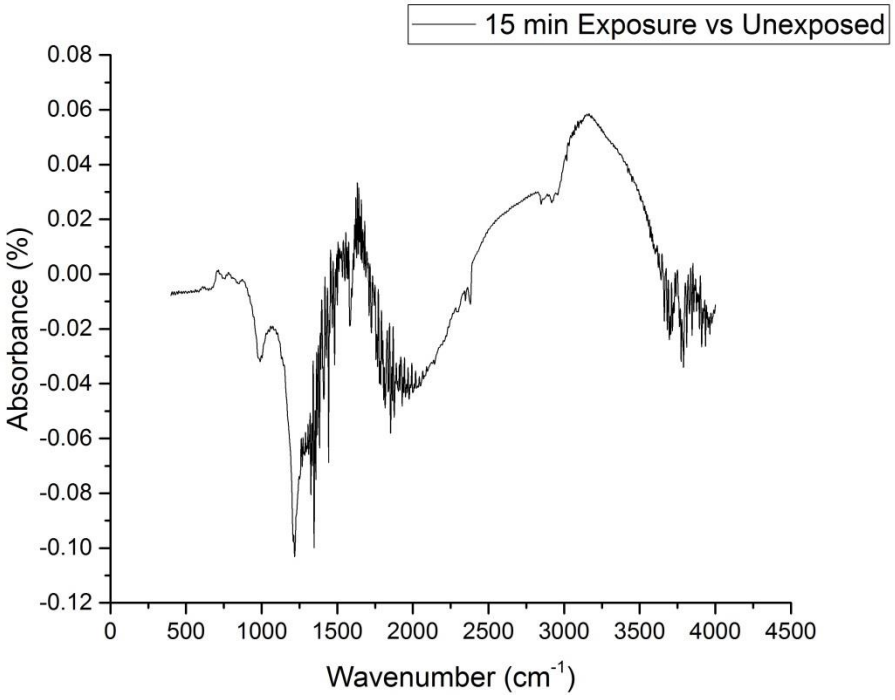

Figure 4.10: FTIR-ATR absorbance spectrum for polymer material coated on glass substrate and exposed to ozone concentration of 600 ppb (±10%) for 15 min with the spectrum from unexposed sample treated as the background

So, the stronger signal from transmission mode was attempted to be utilized in order to gain some meaningful data. Silicon is transparent to infrared light. Hence, the devices were fabricated on Si substrates following the same steps which were used for glass substrates for Part – I, i.e, only the polymer material being exposed to ozone. FTIR measurements were carried out on these devices in the transmission mode. Fig 4.11 below shows the transmission spectrum for the Silicon substrate.

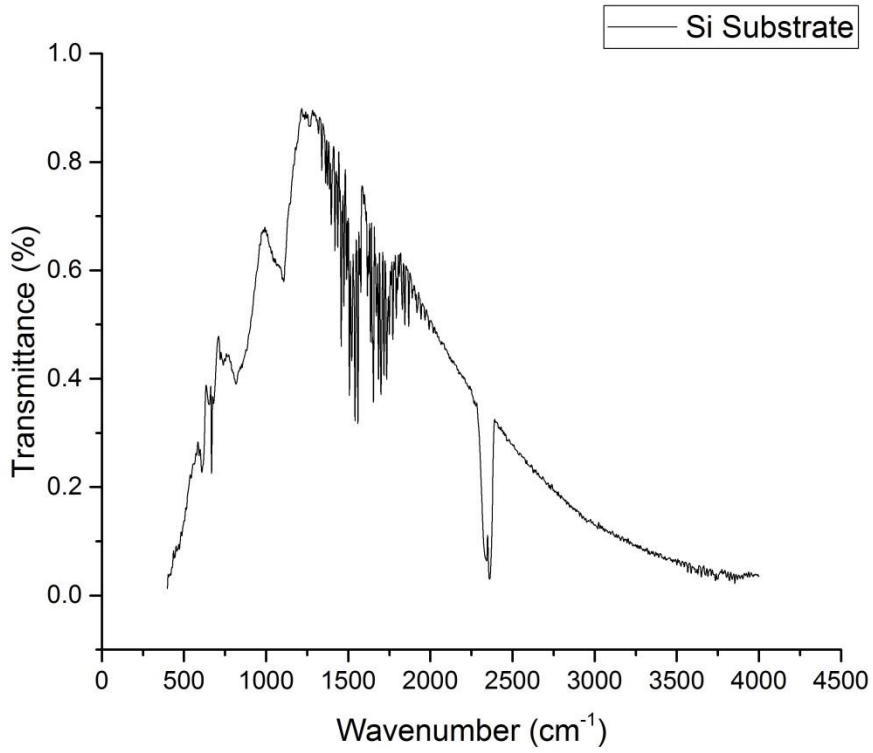

Figure 4.11: FTIR Transmission spectrum for Silicon substrate

Subsequent measurements were carried out on polymer sample coated on Si substrate and unexposed to ozone and the transmission spectrum obtained from this measurement was used as background to measure the transmission spectrum for polymer material coated on Si substrate and exposed to ozone concentration on 600 ppb for 15 min so as to note the difference in transmission peaks due to ozone oxidation.

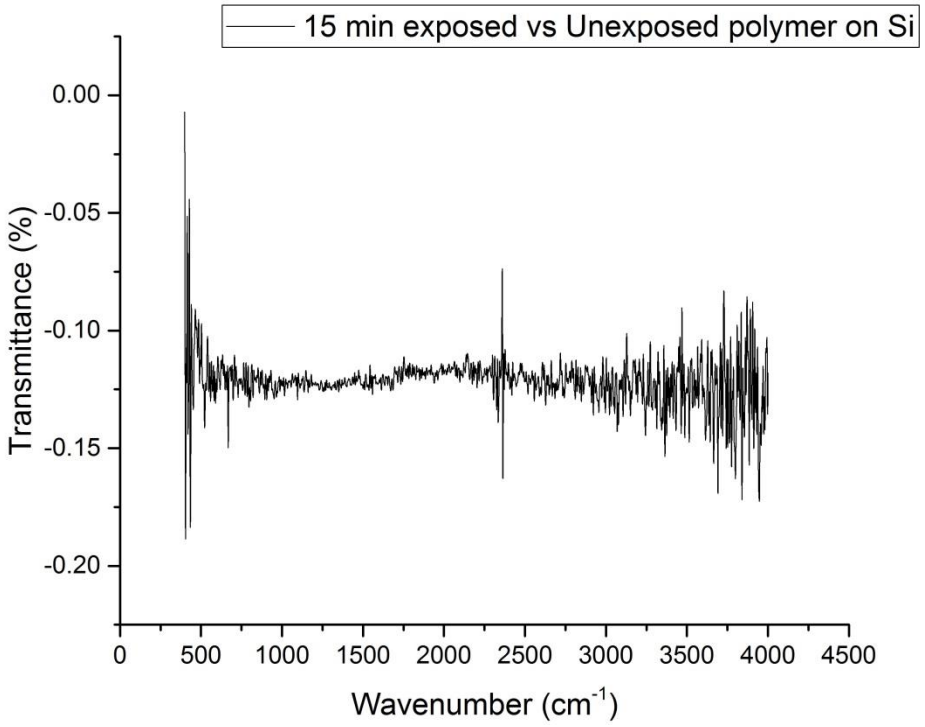

Figure 4.12: FTIR transmission spectrum for polymer material coated on Si substrate and exposed to ozone concentration of 600 ppb (±10%) for 15 min with the spectrum from unexposed sample coated on Si substrate treated as the background

As can be seen from the above Fig 4.12, even this technique of using Si as substrate material leads to considerable amount of noise to obtain any meaningful data regarding the change in transmission peaks of the polymer due to ozone oxidation. One reason for these observations is that the Si substrate used was polished only on the coated side and rough on the other side; hence the roughness on back surface may give rise to scattering and hence noise in the data obtained. Although the major reason for the FTIR measurements not working is that the spot size for a typical FTIR system is about 20 µm. The thickness of polymer films used for this experiment is roughly between 200 and 300 nm. Hence, it makes sense that FTIR readings were not able to exclusively scan the polymer layer only.

5 Conclusions

It has been known that the degradation on organic films and anode are major factors that determine device performance. Hence with these observations, it is concluded that direct exposure of the P3HT:$PC_{71}BM$ material to ozone can damage the OPV film and cause film dysfunction very quickly, and the level of decay is dependent on the time and strength of ozone exposure. While the data suggest that accelerated life testing can be conducted, given that film efficiency decay rate was inversely linear with respect to ozone concentrations from ambient to high levels and given that 100% degradation was achieved in 28 hours at ambient concentrations leads to the suggestion of little marginal gain from accelerated testing. Moreover, when the organic films are coated with anodes (i.e., Al and MoO_3 layers), test findings show complete resistance to ozone oxidation of the OPV device. Therefore, the current design of the complete OPV device shows good resistance to ozone without additional protection or encapsulation. These findings suggests that even in areas experiencing extreme ozone levels, the application of specific anode materials (i.e. Al and MoO_3) can be used to protect OPV from ozone oxidation. This finding has significant bearing with respect to the selection and price of encapsulation material requirements for OPV.

The significant results mentioned above were the short-term milestones for this project funded by the National Science Foundation (NSF). Further work on this project is underway. A couple long-term milestones set are repeating the above experiments under more varied values of ozone concentration and increasing the number of data points on the time scale, so that the degradation mechanism can be closely monitored and understood. Also, the second part of this thesis that is fabrication of complete device, including coating of anode materials before exposure to ozone

has been tested to 42 hours. This test will be carried out for longer times (30 – 60 days) so that any failure can be spotted and also to help gauge the robustness of these devices for long-term use. The work presented in this thesis is the starting point in understanding the effect of ozone exposure on the degradation of polymer thin films and also of how anode materials are able to make the device resistant to ozone oxidation by passivation of the active polymer layers. With the above objective in mind, FTIR characterization of the oxidation products was done in order to understand the change in the chemical structure of the polymer material, hence creating a baseline for the degradation mechanism of ozone exposure. The FTIR, having a minimum spot size of 20 μm is not the right tool to analyze the 200 – 300 nm thick polymer films in question. Hence, characterization of these materials is on-going using a Raman-SEM hybrid system having spot size of 100 nm in order to establish the degradation mechanism which will help gear up these highly efficient and economically viable materials to be available for commercial use without added encapsulation requirement.

The above mentioned work in this thesis, from ozone exposure of polymer material to characterization of the oxidized products is also being carried out on another promising and highly efficient OPV material – PCE10, also known as PBDTTT-EFT and PTB7-Th which has published efficiency values of 9 %. In order to achieve all these long-term milestones detailed above, we hope to receive support from the NSF by renewal of this project.

References

[1] J. Kalowekamo, E. Baker (2009). Estimating the manufacturing cost of purely organic solar cells. Solar Energy 83, 1224 – 1231.

[2] J. Ahmad, K. Bazaka, L.J. Anderson, R.D. White, M.V. Jacob (2013). Materials and methods for encapsulation of OPV: A review. Renewable and Sustainable Energy Rev. 27, 104 – 117.

[3] H. Spanggaard, F.C. Krebs (2004). A brief history of the development of organic and polymeric photovoltaics. Solar Energy Materials and Solar Cells 83, 125 – 146.

[4] M. Adi, T. Yohannes, T. Solomon (2004). Solid-state photoelectrochemical device based on poly(3-hexylthiophene) and an ion conducting polymer electrolyte, amorphous poly(ethylene oxide) complexed with I_3^-/ I^- redox couple. Solar Energy Materials and Solar Cells 83, 201 – 310.

[5] E. Bundgaard, F.C. Krebs (2007). Low band gap polymers for organic photovoltaics. Solar Energy Materials and Solar Cells 91, 954 – 985.

[6] Z. He et al (2012). Enhanced power-conversion efficiency in polymer solar cells using an inverted device structure. Nature Photonics 6, 591 – 595.

[7] S. Bai et al (2012). Inverted organic solar cells based on aqueous processed ZnO interlayers at low temperature. Appl. Phys. Letters 100, 203906.

[8] G. Li, C-W. Chu, V. Shrotriya, J. Huang, Y. Yang (2006). Efficient inverted polymer solar cells. Appl. Phys. Letters 88, 253503.

[9] M.O. Reese, M.S. White, G. Rumbles, D.S. Ginley, S.E. Shaheen (2008). Optimal negative electrodes for poly(3-hexylthiophene) : [6,6]–phenyl C61-butyric acid methyl ester bulk heterojunction photovoltaic devices. Appl. Phys. Letters 92, 053307.

[10] H. Neugebauer, C.J. Brabeca, J.C. Hummelen, R.A.J. Janssen, N.S. Sariciftci (1999). Stability studies and degradation analysis of plastic solar cell materials by FTIR spectroscopy. Synthetic Metals 102, 1002 – 1003.

[11] M. Jorgensen, K. Norrman, F.C. Krebs (2008). Stability/ degradation of polymer solar cells. Solar Energy Materials and Solar Cells 92, 686 – 714.

[12] M.O. Reese et al (2008). Pathways for the degradation of organic photovoltaic P3HT:PCBM based devices. Solar Energy Materials and Solar Cells 92, 746 – 752.

[13] M.T. Lloyd et al (2009). Impact of contact evolution on the shelf life of organic solar cells. J. Mater. Chem. 19 (41), 7638 – 7642.

[14] B.A. Macleod (2015). Stability of inverted organic solar cells with ZnO contact layers deposited from precursor solutions. Energy Environ. Sci. 8, 592 – 601.

[15] J.Y. Kim et al (2007). Efficient tandem polymer solar cells fabricated by all - solution processing. Science 317 (5835), 222 – 225.

[16] Y.M. Chang, C.Y. Leu (2013). Conjugated polyelectrolyte and zinc oxide stacked structure as an interlayer in highly efficient and stable organic photovoltaic cells. J. Mater. Chem. 1, 6446 – 6451.

[17] F. Zhang et al (2011). Recent development of the inverted configuration organic solar cells. Solar Energy Materials and Solar Cells 95, 1785 – 1799.

[18] W. Cai, X. Gong, Y. Cao (2010). Polymer solar cells: Recent development and possible routes for improvement in the performance. Solar Energy Materials and Solar Cells 94, 114 – 127.

[19] H. Hoppe, N. S. Sariciftci (2004). Organic solar cells: An overview. J. Mater. Res. 19 (7), 1924 – 1945.

[20] S. Gunes, H. Neugebauer, N. S. Sariciftci (2007). Conjugated polymer - based organic solar cells. Chem. Rev. 107 (4), 1324 – 1338.